AAS 15-392

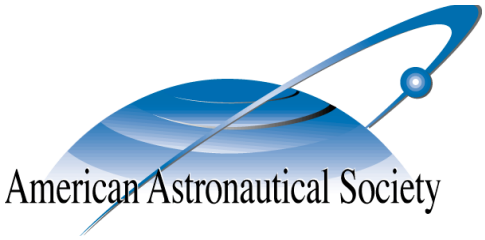

American Institute of
Aeronautics and Astronautics

ON-ORBIT COARSE SUN SENSOR CALIBRATION SENSITIVITY TO SENSOR AND MODEL ERROR

Stephen A. O'Keefe and Hanspeter Schaub

AAS/AIAA Spaceflight Mechanics Meeting

Williamsburg, Virginia **January 11–15, 2015**

AAS Publications Office, P.O. Box 28130, San Diego, CA 92198

AAS 15-392

ON-ORBIT COARSE SUN SENSOR CALIBRATION SENSITIVITY TO SENSOR AND MODEL ERROR

Stephen A. O'Keefe* **and Hanspeter Schaub†**

The size and budgetary limitations of increasingly popular smaller satellites as a lower cost alternative to traditional satellites are a driving factor for making the most of inexpensive components and sensors. One example of an attractive, inexpensive sensor is the coarse cosine-type sun sensor (CSS) that outputs a voltage relative to the input irradiance. CSS are often used, in combination with other sensors, to perform attitude determination. The accuracy of these estimation techniques can be greatly improved by on-orbit calibration of the CSS. However, the requirements for achieving high-accuracy on-orbit calibration can often necessitate significant ground-based support. A Modified Rodrigues Parameter calibration filter, based on an extended consider Kalman filter, that uses an albedo model is presented along with a second filter in which the CSS input due to albedo is treated as a bias. The accuracy of these two methods and their relative computational cost is evaluated. It is found that the estimation schemes are minimally impacted by reduced orbit reference sun-direction accuracy, and that a lower resolution albedo model can significantly reduce computation time without overly sacrificing accuracy.

INTRODUCTION

In recent years there has been a significant increase in interest in smaller satellites as a lower cost alternative to traditional satellites. The size and cost limitations of these satellites are a driving factor for making the most of inexpensive components and sensors. Cosine-type coarse sun sensors (CSS) that output a voltage relative to the input irradiance are an example of such a small, inexpensive sensor. CSS are often used in concert with other sensors[1,2] to perform coarse attitude determination or initially point a spacecraft's solar arrays at the Sun. On-orbit calibration of these sensors can significantly improve the accuracy of attitude estimation techniques,[3] but calibration can involve significant computational and memory requirements.

As noted by Springmann, literature on the on-orbit calibration of sun sensors is sparse.[3] Ortega, López-Rodríguez, et. al., and Wu and Steyn both present calibration of 2-axis sun sensors specific to an individual model.[4,5] Springmann presents a CSS calibration filter capable of calculating CSS scale factor and misalignment.[3] The filter is a quaternion based extended Kalman filter (EKF) approach that assumes the albedo contributions to the EKF Jacobians are small, and the filter performance is shown for flight data.

Presented here are two CSS calibration filters, formulated using Modified Rodrigues Parameters (MRPs) and based on an extended consider Kalman filter (ECKF) approach. A MRP based attitude estimation filter is used here as they have been shown to have equal accuracy to and faster initial

*Graduate Research Assistant, Aerospace Engineering Sciences, University of Colorado, Boulder, CO
†Professor, Aerospace Engineering Sciences, University of Colorado, Boulder, CO, AAS Fellow

convergence than quaternion filters with slightly faster numerical evaluation and simpler coding implementation.[6] An extended consider Kalman filter is used, instead of a traditional EKF, in order to account for known biases in the measurement model. In addition, the impact of the irradiance due to albedo is included to first order in the system Jacobians. The first filter uses an Earth albedo model to estimate the irradiance received by a CSS due to Earth's albedo, whereas the second treats the irradiance due to albedo as an unmodeled bias that is considered. The goal is to compare the relative accuracy and computation time of the two methods in order that the amount of ground-based support required by small satellites may be reduced and autonomy increased.

Numerical simulations are used to demonstrate the performance of the two filters. Significant noise and biases are added to the simulation to make it as realistic as possible. In particular, References 7 and 8 show that simultaneous sun-direction estimation and pointing can be performed when scale factor uncertainties are normally distributed with a standard deviation of $2\,\%$. Here those scale factors are distributed by $30\,\%$, an order of magnitude larger. For comparison, the total solar irradiance only changes by $0.1\,\%$ between minimum and maximum solar activity, and has only changed by $0.09\,\%$ over the last 400 years.[9] Additionally, photodiode calibration is typically on the order of $5\,\%$ for visible light. If calibration to a few percent can be achieved for a large initial uncertainty, such a filter could also be used for autonomous fault detection of CSS as having a good calibration and covariance measure of the CSS would help detect if a sensor is not operating properly.

An overview of the coarse sun sensor model used is presented first, along with a description of the CSS configuration used in this study. The extended consider Kalman filter is briefly reviewed. A full calibration filter formulation is presented followed by a reduced filter in which the irradiance due to albedo is treated as a bias. Finally, the accuracy and computation time of the algorithms are compared and their sensitivity to reduced fidelity orbit knowledge and sun-direction reference model are illustrated through numerical simulation.

COARSE SUN SENSORS

Assuming Lambert's cosine law,[10] the output voltage of an individual CSS can be modeled as

$$V = C\left(\boldsymbol{n}^T \frac{\boldsymbol{s}}{\|\boldsymbol{s}\|} - \frac{F_\alpha}{F_\odot} + \nu_V\right) \tag{1}$$

where $\boldsymbol{n}$ is the unit surface normal of the CSS, $\boldsymbol{s}$ is the sun-direction vector in the body frame, C is a calibration factor, and ν_V is a zero-mean Gaussian random variable included to compensate for sensor noise and model errors. The flux seen by the CSS due to the diffuse reflectance of the Earth is modeled as[1,11]

$$F_\alpha = -\frac{F_\odot}{\pi} \iint_{\boldsymbol{A}} \frac{\alpha}{\|\boldsymbol{r}_{AB}\|^2} \left(\boldsymbol{n}_A^T \frac{\boldsymbol{s}_\oplus}{\|\boldsymbol{s}_\oplus\|}\right) \left(\boldsymbol{n}_A^T \frac{\boldsymbol{r}_{AB}}{\|\boldsymbol{r}_{AB}\|}\right) \left(\boldsymbol{n}^T \frac{\boldsymbol{r}_{AB}}{\|\boldsymbol{r}_{AB}\|}\right) \mathrm{d}A \tag{2}$$

where $F_\odot$ is the solar irradiance in the vicinity of the Earth; $\boldsymbol{A}$ is the surface of the Earth visible to the spacecraft that is also illuminated by the Sun; $\boldsymbol{n}_A$ is the unit normal of a differential area of $\boldsymbol{A}$; $\boldsymbol{s}_\oplus$ is the direction vector from the Earth to the Sun; $\boldsymbol{r}_{AB}$ is a vector from $\mathrm{d}A$ to the body of the spacecraft; and α is the albedo, or reflectivity coefficient, of $\mathrm{d}A$.

The value of the Earth's albedo varies significantly with position, and due to seasonal, ground cover, and cloud cover changes, therefore, daily measurements from 2000 to 2005, corresponding to

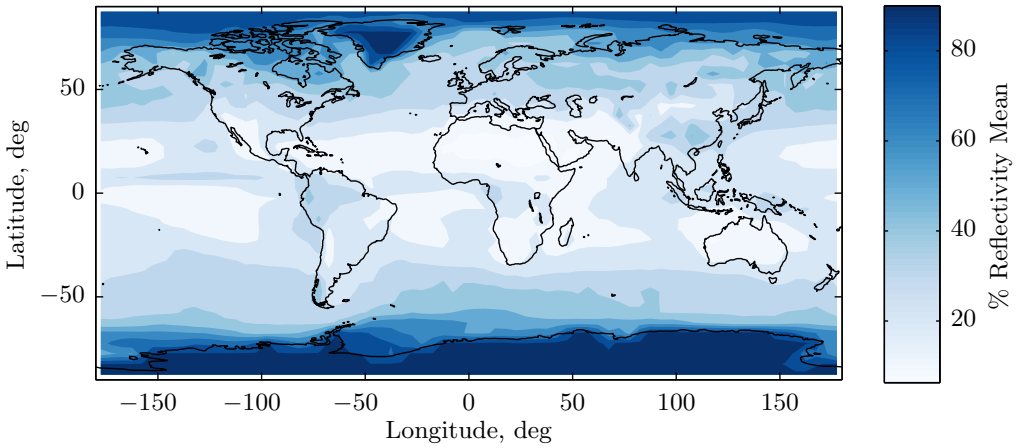

Figure 1: Mean reflectivity of Earth as measured by TOMS mission between 2000 and 2005.

a $1^\circ \times 1.25^\circ$ latitude longitude grid, are used to calculate mean and standard deviation values, shown in Figure 1. The data used in this study to model the Earth's albedo constant were acquired as part of the NASA's Earth-Sun System Division and archived and distributed by the Goddard Earth Sciences (GES) Data and Information Services Center (DISC) Distributed Active Archive Center (DAAC). These values are used to generate statistically accurate values for the Earth's albedo coefficient used in the numerical simulations.

Assuming rotation about the normal of the CSS does not significantly change the output of the sensor*, the true unit direction vector for a CSS can be spherically expressed in the spacecraft body frame as

$$^{\mathcal{B}}\boldsymbol{n} = \begin{bmatrix} \cos(\phi)\cos(\theta) & \cos(\phi)\sin(\theta) & \sin(\phi) \end{bmatrix}^T \tag{3}$$

where θ is the azimuth angle, measured positive from the body $+x$-axis around the $+z$-axis, and ϕ is the elevation angle, measured positive toward the body $+z$-axis from the x-y plane, of the CSS direction vector. Accounting for field of view limitations of actual hardware, Equation (1) becomes

$$V = C\left(V_d + V_\alpha + \nu_V\right)$$

$$V_d = \begin{cases} \boldsymbol{n}^T \frac{\boldsymbol{s}}{\|\boldsymbol{s}\|} & \text{if } \boldsymbol{n}^T \frac{\boldsymbol{s}}{\|\boldsymbol{s}\|} \geq \cos\psi \\ 0 & \text{if } \boldsymbol{n}^T \frac{\boldsymbol{s}}{\|\boldsymbol{s}\|} < \cos\psi \end{cases}$$

$$V_\alpha = \begin{cases} -\frac{1}{\pi} \iint\limits_{\boldsymbol{A}} \frac{\alpha}{\|\boldsymbol{r}_{AB}\|^2} \left(\boldsymbol{n}_A^T \frac{\boldsymbol{s}_\oplus}{\|\boldsymbol{s}_\oplus\|}\right) \left(\boldsymbol{n}_A^T \frac{\boldsymbol{r}_{AB}}{\|\boldsymbol{r}_{AB}\|}\right) \left(\boldsymbol{n}^T \frac{\boldsymbol{r}_{AB}}{\|\boldsymbol{r}_{AB}\|}\right) \mathrm{d}A & \text{if } B \notin \boldsymbol{\mathcal{S}} \\ 0 & \text{if } B \in \boldsymbol{\mathcal{S}} \end{cases} \tag{4}$$

where ψ is the half angle of the CSS field of view, B is the spacecraft's position in orbit, and $\boldsymbol{\mathcal{S}}$ is the region of the spacecraft's orbit in the shadow of the Earth.

The spacecraft used for this study is assumed to be equipped with eight cosine-type CSS in a dual pyramid configuration. Eight sensors with 120° edge-to-edge fields of view are arranged on

*Test data from a heliostat shows there is some variability in the output of a sensor corresponding to rotation about the normal vector of the CSS; however, the magnitude of this variability is small.

the $+z$ and $-z$ faces of the spacecraft oriented 90° apart and angled 45° from the body z axis. The $-z$ facing sensors are rotated by 45° about the z axis with respect to the $+z$ facing sensors. An illustration of this configuration is shown in Figure 2a.

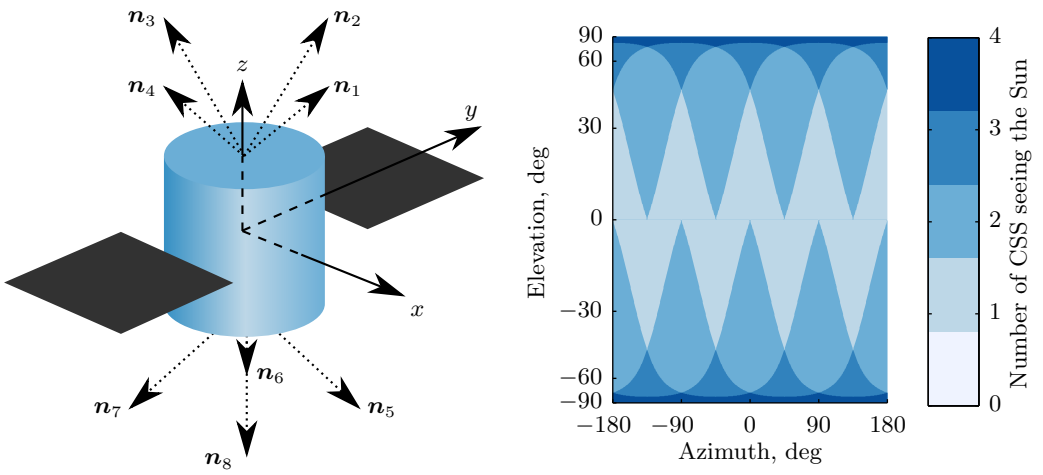

(a) Schematic of spacecraft.

(b) CSS coverage map.

Figure 2: Illustration of spacecraft, with CSS unit vectors, for an offset dual pyramid configuration and the associated coverage map.

Figure 2b shows the number of CSS to which the Sun is visible for any relation of the Sun with respect to the spacecraft. Note that the fields of view of the CSS are clipped at the local-horizontal plane by the spacecraft structure and solar panel arrays. A Lambert cylindrical area preserving projection[12] is used so as to give a fair relative area comparison of the regions of coverage.

COARSE SUN SENSOR CALIBRATION

It has been shown that CSS can be calibrated to account for scale factor and alignment errors using a quaternion based EKF.[3] However, this approach is computed by ground-based support using a ground-based orbit solution. In order to reduce mission costs it would be highly valuable if such calibration could be carried out autonomously on-board a spacecraft. With the computational and memory limitations of small satellites it is important to consider the level of accuracy needed and use an appropriate estimation technique. An overview of the continuous-discrete extended consider Kalman filter is presented, followed by the equations specific to this application for both a full and reduced calibration filter.

Continuous-Discrete Extended Consider Kalman Filter

Initially presented by Schmidt,[13] the consider Kalman filter formulation here is adapted from References 14 and 15. Consider a system with the augmented state vector given by

$$\boldsymbol{z}(t) = \begin{bmatrix} \boldsymbol{x}(t) \\ \boldsymbol{\beta}_\eta(t) \\ \boldsymbol{\beta}_\nu(t) \end{bmatrix} \tag{5}$$

where $\boldsymbol{x}$ is the vector of states to be estimated, $\boldsymbol{\beta}_\eta$ is a random zero-mean constant dynamic model bias with

$$\mathrm{E}\left[\left(\hat{\boldsymbol{\beta}}_\eta(t)-\boldsymbol{\beta}_\eta(t)\right)\left(\hat{\boldsymbol{\beta}}_\eta(\tau)-\boldsymbol{\beta}_\eta(\tau)\right)^T\right]=\boldsymbol{B}_\eta(t)\,\delta\left(t-\tau\right) \tag{6a}$$

$$\mathrm{E}\left[\left(\hat{\boldsymbol{x}}(t)-\boldsymbol{x}(t)\right)\left(\hat{\boldsymbol{\beta}}_\eta(\tau)-\boldsymbol{\beta}_\eta(\tau)\right)^T\right]=\boldsymbol{L}(t)\,\delta\left(t-\tau\right) \tag{6b}$$

and $\boldsymbol{\beta}_\nu$ is a random zero-mean constant measurement equation bias with

$$\mathrm{E}\left[\left(\hat{\boldsymbol{\beta}}_\nu(t)-\boldsymbol{\beta}_\nu(t)\right)\left(\hat{\boldsymbol{\beta}}_\nu(\tau)-\boldsymbol{\beta}_\nu(\tau)\right)^T\right]=\boldsymbol{B}_\nu(t)\,\delta\left(t-\tau\right) \tag{7a}$$

$$\mathrm{E}\left[\left(\hat{\boldsymbol{x}}(t)-\boldsymbol{x}(t)\right)\left(\hat{\boldsymbol{\beta}}_\nu(\tau)-\boldsymbol{\beta}_\nu(\tau)\right)^T\right]=\boldsymbol{\Lambda}(t)\,\delta\left(t-\tau\right). \tag{7b}$$

It is assumed the bias vectors are uncorrelated with either the measurement or dynamic process noise. Similar to the augmented state vector, the covariance matrix can be written in block form as

$$\boldsymbol{P}_z(t)=\mathrm{E}\left[\left(\hat{\boldsymbol{z}}(t)-\boldsymbol{z}(t)\right)\left(\hat{\boldsymbol{z}}(t)-\boldsymbol{z}(t)\right)^T\right]=\begin{bmatrix}\boldsymbol{P}_x(t) & \boldsymbol{L}(t) & \boldsymbol{\Lambda}(t)\\ \boldsymbol{L}^T(t) & \boldsymbol{B}_\eta(t) & \boldsymbol{0}\\ \boldsymbol{\Lambda}^T(t) & \boldsymbol{0} & \boldsymbol{B}_\nu(t)\end{bmatrix}. \tag{8}$$

The continuous-time state dynamics are assumed to be of the form

$$\dot{\boldsymbol{z}}(t)=\boldsymbol{f}(\boldsymbol{z}(t)\,,\boldsymbol{u}(t)\,,\boldsymbol{\eta}(t)\,,t) \tag{9}$$

where $\boldsymbol{u}(t)$ is the control input, $\boldsymbol{\eta}(t)$ is continuous-time zero-mean white Gaussian process noise with spectral density $\boldsymbol{Q}(t)$. The state covariance propagation equations are written as

$$\dot{\boldsymbol{P}}_x(t)=\boldsymbol{F}(t)\,\boldsymbol{P}_x(t)+\boldsymbol{P}_x(t)\,\boldsymbol{F}^T(t)+\boldsymbol{S}(t)\,\boldsymbol{L}^T(t)+\boldsymbol{L}(t)\,\boldsymbol{S}^T(t)+\boldsymbol{G}(t)\,\boldsymbol{Q}(t)\,\boldsymbol{G}^T(t) \tag{10a}$$

$$\dot{\boldsymbol{L}}(t)=\boldsymbol{F}(t)\,\boldsymbol{L}(t)+\boldsymbol{S}(t)\,\boldsymbol{B}_\eta(t) \tag{10b}$$

$$\dot{\boldsymbol{\Lambda}}(t)=\boldsymbol{F}(t)\,\boldsymbol{\Lambda}(t) \tag{10c}$$

$$\dot{\boldsymbol{B}}_\eta=\boldsymbol{0} \tag{10d}$$

$$\dot{\boldsymbol{B}}_\nu=\boldsymbol{0} \tag{10e}$$

where

$$\boldsymbol{F}(t)=\left.\frac{\partial\boldsymbol{f}}{\partial\boldsymbol{x}}\right|_{\hat{\boldsymbol{z}},\hat{\boldsymbol{\beta}}_\eta,\boldsymbol{u}},\quad \boldsymbol{S}(t)=\left.\frac{\partial\boldsymbol{f}}{\partial\boldsymbol{\beta}_\eta}\right|_{\hat{\boldsymbol{z}},\hat{\boldsymbol{\beta}}_\eta,\boldsymbol{u}},\quad \boldsymbol{G}(t)=\left.\frac{\partial\boldsymbol{f}}{\partial\boldsymbol{\eta}}\right|_{\hat{\boldsymbol{z}},\hat{\boldsymbol{\beta}}_\eta,\boldsymbol{u}}. \tag{11}$$

The discrete-time measurements are assumed to be of the form

$$\boldsymbol{y}_k=\boldsymbol{h}(\boldsymbol{z}_k,\boldsymbol{u}_k,\boldsymbol{\nu}_k,t_k) \tag{12}$$

where $\boldsymbol{\nu}_k$ is discrete-time zero-mean Gaussian white-noise with covariance $\boldsymbol{R}_k$. The measurement update equations are given by

$$\boldsymbol{P}_{x,k}^+=\boldsymbol{P}_{x,k}^--\boldsymbol{K}_{x,k}^*\boldsymbol{W}_k\boldsymbol{K}_{x,k}^{*T} \tag{13a}$$

$$\boldsymbol{L}_k^+=\left(\boldsymbol{I}-\boldsymbol{K}_{x,k}^*\boldsymbol{H}_k\right)\boldsymbol{L}_k^- \tag{13b}$$

$$\boldsymbol{\Lambda}_k^+=\left(\boldsymbol{I}-\boldsymbol{K}_{x,k}^*\boldsymbol{H}_k\right)\boldsymbol{\Lambda}_k^--\boldsymbol{K}_{x,k}^*\boldsymbol{J}_k\boldsymbol{B}_\nu \tag{13c}$$

$$\boldsymbol{B}_\eta^+=\boldsymbol{B}_\eta^- \tag{13d}$$

$$\boldsymbol{B}_\nu^+=\boldsymbol{B}_\nu^- \tag{13e}$$

where

$$\boldsymbol{H}_k = \left.\frac{\partial \boldsymbol{h}_k}{\partial \boldsymbol{x}_k}\right|_{\hat{\boldsymbol{x}}_k^-, \hat{\boldsymbol{\beta}}_{\nu,k}^-}, \quad \boldsymbol{J}_k = \left.\frac{\partial \boldsymbol{h}_k}{\partial \boldsymbol{\beta}_\nu}\right|_{\hat{\boldsymbol{x}}_k^-, \hat{\boldsymbol{\beta}}_{\nu,k}^-}, \quad \boldsymbol{M}_k = \left.\frac{\partial \boldsymbol{h}_k}{\partial \boldsymbol{\nu}_k}\right|_{\hat{\boldsymbol{x}}_k^-, \hat{\boldsymbol{\beta}}_{\nu,k}^-} \tag{14}$$

and

$$\boldsymbol{K}_{x,k}^* = \left(\boldsymbol{P}_{x,k}^- \boldsymbol{H}_k^T + \boldsymbol{\Lambda}_k^- \boldsymbol{J}_k^T\right) \boldsymbol{W}^{-1} \tag{15a}$$

$$\boldsymbol{W}_k = \boldsymbol{H}_k \boldsymbol{P}_{x,k}^- \boldsymbol{H}_k^T + \boldsymbol{J}_k \left(\boldsymbol{\Lambda}_k^-\right)^T \boldsymbol{H}_k^T + \boldsymbol{H}_k \boldsymbol{\Lambda}_k^- \boldsymbol{J}_k^T + \boldsymbol{J}_k \boldsymbol{B}_\nu \boldsymbol{J}_k^T + \boldsymbol{M}_k \boldsymbol{R}_k \boldsymbol{M}_k^T. \tag{15b}$$

Full CSS Calibration Filter

The full CSS calibration filter assumes the spacecraft has CSS, inertial attitude, and angular rate measurements available, as well as an orbit solution and an estimate of the reference Earth-Sun vector. The calculation of the reference Earth-Sun vector requires the current Julian date. The state vector and process noise vectors are set to

$$\boldsymbol{x}(t) = \begin{bmatrix} \boldsymbol{\sigma}(t) \\ {}^{\mathcal{G}}\boldsymbol{\omega}_\beta(t) \\ \boldsymbol{C}(t) \\ \boldsymbol{\theta} \\ \boldsymbol{\phi} \end{bmatrix}, \quad \boldsymbol{\eta}(t) = \begin{bmatrix} {}^{\mathcal{G}}\boldsymbol{\eta}_\omega(t) \\ {}^{\mathcal{G}}\boldsymbol{\eta}_{\omega_\beta}(t) \\ \boldsymbol{\eta}_C(t) \end{bmatrix} \tag{16}$$

where $\boldsymbol{\sigma}(t)$ is the MRP attitude description of the spacecraft, $\boldsymbol{\theta}$ is a vector of CSS azimuth angles, and $\boldsymbol{\phi}$ is a vector of CSS elevation angles.

The rate gyro measurement are assumed to follow Farrenkopf's approximation[16]

$${}^{\mathcal{G}}\tilde{\boldsymbol{\omega}}(t) = [BG]\left({}^{\mathcal{G}}\boldsymbol{\omega}(t) + {}^{\mathcal{G}}\boldsymbol{\omega}_\beta(t) + {}^{\mathcal{G}}\boldsymbol{\eta}_\omega(t)\right) \tag{17a}$$

$$\dot{\boldsymbol{\omega}}_\beta(t) = \boldsymbol{\eta}_{\omega_\beta}(t) \tag{17b}$$

where a left superscript $\mathcal{G}$ indicates a quantity expressed in the rate gyro frame; $[BG]$ is the DCM describing the rotation from the rate gyro frame to the spacecraft body frame; $\tilde{\boldsymbol{\omega}}(t)$ is the sensed angular velocity; $\boldsymbol{\omega}(t)$ is the true angular velocity; $\boldsymbol{\omega}_\beta(t)$ is the measurement bias drift, modeled as a rate random walk process; and $\boldsymbol{\eta}_\omega(t)$ and $\boldsymbol{\eta}_{\omega_\beta}(t)$ are zero-mean Gaussian rate and angular acceleration, respectively, white-noise processes.

The MRP dynamics are given by

$$\dot{\boldsymbol{\sigma}}(t) = \frac{1}{4}\left[B(\boldsymbol{\sigma}(t))\right][BG]\left({}^{\mathcal{G}}\tilde{\boldsymbol{\omega}}(t) - {}^{\mathcal{G}}\boldsymbol{\omega}_\beta(t) - {}^{\mathcal{G}}\boldsymbol{\eta}_\omega(t)\right) \tag{18}$$

where

$$[B(\boldsymbol{\sigma})] = \left[\left(1 - \boldsymbol{\sigma}^T\boldsymbol{\sigma}\right)\left[\boldsymbol{I}_{3\times 3}\right] + 2\left[\boldsymbol{\sigma}\right]_\times + 2\boldsymbol{\sigma}\boldsymbol{\sigma}^T\right]. \tag{19}$$

The individual sensor calibration factors $\boldsymbol{C}(t)$ are assumed to be governed by

$$\dot{\boldsymbol{C}}(t) = \boldsymbol{\eta}_C(t). \tag{20}$$

It is expected over time the values of $\boldsymbol{C}$ will slowly decrease as CSS degrade due to radiation. For short time scales it is expected to remain constant and is modeled as having a random walk as a

worst case analysis. Defining the best estimate of the true spacecraft angular velocity in the body frame as

$$^{\mathcal{B}}\hat{\boldsymbol{\omega}}(t) = [BG]\left(^{\mathcal{G}}\tilde{\boldsymbol{\omega}}(t) - {}^{\mathcal{G}}\hat{\boldsymbol{\omega}}_b(t)\right) \tag{21}$$

the pertinent propagation Jacobians are given by

$$\boldsymbol{F}(t) = \begin{bmatrix} \frac{1}{2}\left(\hat{\boldsymbol{\sigma}}\,^{\mathcal{B}}\hat{\boldsymbol{\omega}}^T + {}^{\mathcal{B}}\hat{\boldsymbol{\omega}}\hat{\boldsymbol{\sigma}}^T - \left[{}^{\mathcal{B}}\hat{\boldsymbol{\omega}}\right]_\times + \hat{\boldsymbol{\sigma}}^T\,^{\mathcal{B}}\hat{\boldsymbol{\omega}}\boldsymbol{I}_{3\times3}\right) & -\frac{1}{4}\left[B(\boldsymbol{\sigma})\right][BG] & \boldsymbol{0}_{3\times3N} \\ \boldsymbol{0}_{(3+3N)\times3} & \boldsymbol{0}_{(3+3N)\times3} & \boldsymbol{0}_{(3+3N)\times3N} \end{bmatrix} \tag{22a}$$

$$\boldsymbol{G}(t) = \begin{bmatrix} -\frac{1}{4}\left[B(\boldsymbol{\sigma})\right][BG] & \boldsymbol{0}_{3\times3} & \boldsymbol{0}_{3\times N} \\ \boldsymbol{0}_{3\times3} & \boldsymbol{I}_{3\times3} & \boldsymbol{0}_{3\times N} \\ \boldsymbol{0}_{N\times3} & \boldsymbol{0}_{N\times3} & \boldsymbol{I}_{N\times N} \\ \boldsymbol{0}_{2N\times3} & \boldsymbol{0}_{2N\times3} & \boldsymbol{0}_{2N\times N} \end{bmatrix} \tag{22b}$$

where $\hat{\boldsymbol{\sigma}}$ is the current best estimate of the attitude MRP, and N is the total number of CSS. The block structure of the Jacobians, particularly the sections equal to zero, should be noted when implementing the state update in order to reduce the total computations necessary.

As noted previously, it is assumed direct measurements of the body's attitude, via a star tracker or other generic attitude sensor, are available in addition to CSS measurements. Because these measurements may be sampled at different frequencies, and their noise values are uncorrelated, they are presented here as separate measurement updates.

The attitude measurements are modeled by

$$\boldsymbol{y}_k = \boldsymbol{\sigma}_k + \boldsymbol{\nu}_{\sigma,k} \tag{23}$$

where $\boldsymbol{\nu}_{\sigma,k}$ is discrete-time white noise with covariance $\boldsymbol{R}_{\sigma,k}$. The measurement update Jacobians for these attitude measurements are given by

$$\boldsymbol{H}_k = \begin{bmatrix} \boldsymbol{I}_{3\times3} & \boldsymbol{0}_{3\times(3+3N)} \end{bmatrix}, \quad \boldsymbol{J}_k = \boldsymbol{0}, \quad \boldsymbol{M}_k = \boldsymbol{I}_{3\times3}. \tag{24a}$$

The CSS measurement model given by Equation (4) is modified so that it is written in terms of the chosen state vector. It is assumed that the spacecraft has some estimate of the Earth-Sun vector $\boldsymbol{s}_\oplus$ and its own position relative to the Earth $\boldsymbol{r}_B$. The actual sun-direction vector can be written as

$$^{\mathcal{B}}\boldsymbol{s} = [BN]\,^{\mathcal{N}}\left(\boldsymbol{s}_\oplus - \boldsymbol{r}_B\right) \tag{25}$$

where $\boldsymbol{r}_B$ is the actual position of the spacecraft relative to the Earth, $\boldsymbol{s}_\oplus$ is the actual direction vector from the Earth to the Sun, and the direction cosine matrix $[BN]$ is written in terms of the attitude MRP as

$$[BN] = \left[I_{3\times3}\right] + \frac{8\left[\boldsymbol{\sigma}\right]_\times^2 - 4\left(1-\sigma^2\right)\left[\boldsymbol{\sigma}\right]_\times}{\left(1+\sigma^2\right)^2} \tag{26}$$

where $\sigma^{2n} = \left(\boldsymbol{\sigma}^T\boldsymbol{\sigma}\right)^n$. Because the estimation algorithm is assumed to only have estimates of the spacecraft position and Earth-Sun reference vector, the best estimate of the sun-direction vector is given by

$$^{\mathcal{B}}\hat{\boldsymbol{s}} = [BN]\,^{\mathcal{N}}\left(\hat{\boldsymbol{s}}_\oplus - \hat{\boldsymbol{r}}_B\right) \tag{27}$$

where $\boldsymbol{r}_B = \hat{\boldsymbol{r}}_B - \boldsymbol{r}_{B_\beta}$, $\boldsymbol{r}_{B_\beta}$ is a bias in the uncertainty in the spacecraft position with

$$\begin{aligned} \mathrm{E}\Big[\Big(\hat{\boldsymbol{r}}_{B_\beta} - \boldsymbol{r}_{B_\beta}\Big)\Big] &= \boldsymbol{0}, \\ \mathrm{E}\Big[\Big(\hat{\boldsymbol{r}}_{B_\beta} - \boldsymbol{r}_{B_\beta}\Big)\Big(\hat{\boldsymbol{r}}_{B_\beta} - \boldsymbol{r}_{B_\beta}\Big)^T\Big] &= \boldsymbol{B}_{r_B,k}\delta_{jk}\;\forall\, j,k \end{aligned} \tag{28}$$

$\boldsymbol{s}_\oplus = \hat{\boldsymbol{s}}_\oplus - \boldsymbol{s}_{\oplus_\beta}$, and $\boldsymbol{s}_{\oplus_\beta}$ is a measurement bias due to model errors in the reference Earth-Sun vector with

$$\begin{aligned} \mathrm{E}\Big[\Big(\hat{\boldsymbol{s}}_{\oplus_\beta,k} - \boldsymbol{s}_{\oplus_\beta,k}\Big)\Big] &= \boldsymbol{0}, \\ \mathrm{E}\Big[\Big(\hat{\boldsymbol{s}}_{\oplus_\beta,k} - \boldsymbol{s}_{\oplus_\beta,k}\Big)\Big(\hat{\boldsymbol{s}}_{\oplus_\beta,k} - \boldsymbol{s}_{\oplus_\beta,k}\Big)^T\Big] &= \boldsymbol{B}_{s_\oplus,k}\delta_{jk}\;\forall\, j,k. \end{aligned} \tag{29}$$

The error in a properly post-processed orbit solution will most likely resemble white noise. However, the error in a real time propagation of the spacecraft position will more likely exhibit bias-like characteristics and so it is treated as such.

The vector from the differential area to the spacecraft is written as

$$^{\mathcal{N}}\boldsymbol{r}_{AB} = {}^{\mathcal{N}}\boldsymbol{r}_B - {}^{\mathcal{N}}\boldsymbol{r}_A \tag{30}$$

and the best estimate of this vector is given by

$$^{\mathcal{N}}\hat{\boldsymbol{r}}_{AB} = {}^{\mathcal{N}}\hat{\boldsymbol{r}}_B - {}^{\mathcal{N}}\boldsymbol{r}_A \tag{31}$$

using the definitions given previously.

Substituting into Equation (4) gives

$$V = C\left(V_d + V_\alpha + \nu_V\right)$$

$$V_d = \begin{cases} {}^{\mathcal{B}}\Big[\cos\phi\cos\theta \quad \cos\phi\sin\theta \quad \sin\phi\Big]\,[BN]\,\frac{{}^{\mathcal{N}}\boldsymbol{s}_\oplus - {}^{\mathcal{N}}\boldsymbol{r}_B}{\left\|{}^{\mathcal{N}}\boldsymbol{s}_\oplus - {}^{\mathcal{N}}\boldsymbol{r}_B\right\|} & \text{if } \boldsymbol{n}^T\frac{\boldsymbol{s}}{\|\boldsymbol{s}\|} \geq \cos\psi \\ 0 & \text{if } \boldsymbol{n}^T\frac{\boldsymbol{s}}{\|\boldsymbol{s}\|} < \cos\psi \end{cases}$$

$$V_\alpha = \begin{cases} -\frac{1}{\pi}\iint\limits_{\boldsymbol{A}} (\alpha+\nu_\alpha)\,\frac{{}^{\mathcal{N}}\boldsymbol{n}_A^T\,{}^{\mathcal{N}}\boldsymbol{s}_\oplus}{\left\|{}^{\mathcal{N}}\boldsymbol{r}_{AB}\right\|^2\left\|{}^{\mathcal{N}}\boldsymbol{s}_\oplus\right\|}\left({}^{\mathcal{N}}\boldsymbol{n}_A^T\frac{{}^{\mathcal{N}}\boldsymbol{r}_{AB}}{\left\|{}^{\mathcal{N}}\boldsymbol{r}_{AB}\right\|}\right) \\ \qquad * \left({}^{\mathcal{B}}\Big[\cos\phi\cos\theta \quad \cos\phi\sin\theta \quad \sin\phi\Big]\,[BN]\,\frac{{}^{\mathcal{N}}\boldsymbol{r}_{AB}}{\left\|{}^{\mathcal{N}}\boldsymbol{r}_{AB}\right\|}\right)\mathrm{d}A & \text{if } B \notin \boldsymbol{\mathcal{S}} \\ 0 & \text{if } B \in \boldsymbol{\mathcal{S}} \end{cases} \tag{32}$$

where ν_α is zero-mean Gaussian noise representing the uncertainty in the albedo coefficient of $\mathrm{d}A$ calculated from the NASA TOMS data. Defining the measurement noise and bias vectors as

$$\boldsymbol{\nu}_k = \begin{bmatrix} \boldsymbol{\nu}_{V,k} \\ \boldsymbol{\nu}_{\alpha,k} \end{bmatrix}, \quad \boldsymbol{\beta}_\nu = \begin{bmatrix} {}^{\mathcal{N}}\boldsymbol{s}_{\oplus_\beta,k} \\ {}^{\mathcal{N}}\boldsymbol{r}_{B_\beta,k} \end{bmatrix} \tag{33}$$

where $\boldsymbol{\nu}_{\alpha,k}$ is vector, of length N_α, of all the albedo coefficient uncertainty terms in $\boldsymbol{A}$, the measurement update Jacobians are given by

$$\boldsymbol{H}_k = \boldsymbol{H}_{d,k} + \boldsymbol{H}_{\alpha,k} \tag{34a}$$

$$\boldsymbol{H}_{d,k} = \begin{bmatrix} \begin{bmatrix} \boldsymbol{a}_{1,k} \\ \vdots \\ \boldsymbol{a}_{N,k} \end{bmatrix} & \boldsymbol{0}_{N\times 3} & \operatorname{diag}\Big(b_{1,k},\dots,b_{N,k}\Big) & \operatorname{diag}\Big(c_{1,k},\dots,c_{N,k}\Big) & \operatorname{diag}\Big(d_{1,k},\dots,d_{N,k}\Big) \end{bmatrix}$$

$$(\cdot)_{i,k} = \begin{cases} (\bar{\cdot})_{i,k} & \text{if } \frac{\boldsymbol{n}_i^T \hat{\boldsymbol{s}}_k}{\|\boldsymbol{n}_i\|\|\hat{\boldsymbol{s}}_k\|} \geq \cos\psi_i \\ \boldsymbol{0} & \text{if } \frac{\boldsymbol{n}_i^T \hat{\boldsymbol{s}}_k}{\|\boldsymbol{n}_i\|\|\hat{\boldsymbol{s}}_k\|} < \cos\psi_i \end{cases}$$

$$\bar{\boldsymbol{a}}_{i,k} = \hat{C}_{i,k}{}^{\mathcal{B}}\big[\cos\phi_i\cos\theta_i \quad \cos\phi_i\sin\theta_i \quad \sin\phi_i\big] \frac{\partial}{\partial\boldsymbol{\sigma}} \left([BN] \frac{{}^{\mathcal{N}}\hat{\boldsymbol{s}}_k}{\|{}^{\mathcal{N}}\hat{\boldsymbol{s}}_k\|} \right)\Bigg|_{\hat{\boldsymbol{\sigma}}_k}$$

$$\bar{b}_{i,k} = {}^{\mathcal{B}}\big[\cos\phi_i\cos\theta_i \quad \cos\phi_i\sin\theta_i \quad \sin\phi_i\big] [BN] \frac{{}^{\mathcal{N}}\hat{\boldsymbol{s}}_k}{\|{}^{\mathcal{N}}\hat{\boldsymbol{s}}_k\|}$$

$$\bar{c}_{i,k} = \hat{C}_{i,k}{}^{\mathcal{B}}\big[-\cos\phi_i\sin\theta_i \quad \cos\phi_i\cos\theta_i \quad 0\big] [BN] \frac{{}^{\mathcal{N}}\hat{\boldsymbol{s}}_k}{\|{}^{\mathcal{N}}\hat{\boldsymbol{s}}_k\|}$$

$$\bar{d}_{i,k} = \hat{C}_{i,k}{}^{\mathcal{B}}\big[-\sin\phi_i\cos\theta_i \quad -\sin\phi_i\sin\theta_i \quad \cos\phi_i\big] [BN] \frac{{}^{\mathcal{N}}\hat{\boldsymbol{s}}_k}{\|{}^{\mathcal{N}}\hat{\boldsymbol{s}}_k\|} \tag{34b}$$

$$\boldsymbol{H}_{\alpha,k} = \begin{bmatrix} \begin{bmatrix} \boldsymbol{a}_{1,k} \\ \vdots \\ \boldsymbol{a}_{N,k} \end{bmatrix} & \boldsymbol{0}_{N\times 3} & \operatorname{diag}\Big(b_{1,k},\dots,b_{N,k}\Big) & \operatorname{diag}\Big(c_{1,k},\dots,c_{N,k}\Big) & \operatorname{diag}\Big(d_{1,k},\dots,d_{N,k}\Big) \end{bmatrix}$$

$$(\cdot)_{i,k} = \begin{cases} (\bar{\cdot})_{i,k} & \text{if } B \notin \boldsymbol{\mathcal{S}} \\ \boldsymbol{0} & \text{if } B \in \boldsymbol{\mathcal{S}} \end{cases}, \quad \varrho = \frac{\alpha^{\mathcal{N}}\boldsymbol{n}_A^{T\,\mathcal{N}}\hat{\boldsymbol{s}}_\oplus}{\|{}^{\mathcal{N}}\hat{\boldsymbol{r}}_{AB,k}\|^2\|{}^{\mathcal{N}}\hat{\boldsymbol{s}}_\oplus\|} \left({}^{\mathcal{N}}\boldsymbol{n}_A^T \frac{{}^{\mathcal{N}}\hat{\boldsymbol{r}}_{AB,k}}{\|{}^{\mathcal{N}}\hat{\boldsymbol{r}}_{AB,k}\|} \right)$$

$$\bar{\boldsymbol{a}}_{i,k} \approx -\frac{\hat{C}_{i,k}}{\pi} \iint_{\boldsymbol{A}} \varrho \left({}^{\mathcal{B}}\big[\cos\phi_i\cos\theta_i \quad \cos\phi_i\sin\theta_i \quad \sin\phi_i\big] \frac{\partial}{\partial\boldsymbol{\sigma}} \left([BN] \frac{{}^{\mathcal{N}}\hat{\boldsymbol{r}}_{AB,k}}{\|{}^{\mathcal{N}}\hat{\boldsymbol{r}}_{AB,k}\|} \right)\Bigg|_{\hat{\boldsymbol{\sigma}}_k} \right) \mathrm{d}A$$

$$\bar{b}_{i,k} = -\frac{1}{\pi} \iint_{\boldsymbol{A}} \varrho \left({}^{\mathcal{B}}\big[\cos\phi_i\cos\theta_i \quad \cos\phi_i\sin\theta_i \quad \sin\phi_i\big] [BN] \frac{{}^{\mathcal{N}}\hat{\boldsymbol{r}}_{AB,k}}{\|{}^{\mathcal{N}}\hat{\boldsymbol{r}}_{AB,k}\|} \right) \mathrm{d}A$$

$$\bar{c}_{i,k} \approx -\frac{\hat{C}_{i,k}}{\pi} \iint_{\boldsymbol{A}} \varrho \left({}^{\mathcal{B}}\big[-\cos\phi_i\sin\theta_i \quad \cos\phi_i\cos\theta_i \quad 0\big] [BN] \frac{{}^{\mathcal{N}}\hat{\boldsymbol{r}}_{AB,k}}{\|{}^{\mathcal{N}}\hat{\boldsymbol{r}}_{AB,k}\|} \right) \mathrm{d}A$$

$$\bar{d}_{i,k} \approx -\frac{\hat{C}_{i,k}}{\pi} \iint_{\boldsymbol{A}} \varrho \left({}^{\mathcal{B}}\big[-\sin\phi_i\cos\theta_i \quad -\sin\phi_i\sin\theta_i \quad \cos\phi_i\big] [BN] \frac{{}^{\mathcal{N}}\hat{\boldsymbol{r}}_{AB,k}}{\|{}^{\mathcal{N}}\hat{\boldsymbol{r}}_{AB,k}\|} \right) \mathrm{d}A \tag{34c}$$

$$\boldsymbol{M}_k = \boldsymbol{M}_{\alpha_k} + \Big[\operatorname{diag}\Big(\hat{\boldsymbol{C}}_k^T\Big) \quad \boldsymbol{0}_{N\times N_\alpha}\Big] \tag{35a}$$

$$\boldsymbol{M}_{\alpha,k} = \begin{bmatrix} \boldsymbol{0}_{N\times N} & \boldsymbol{\mathcal{L}}_k \end{bmatrix}$$

$$\mathcal{L}_{ij,k} = \begin{cases} -\frac{\hat{C}_{i,k}}{\pi} \frac{{}^{\mathcal{N}}\boldsymbol{n}_{A_j}^T \, {}^{\mathcal{N}}\hat{\boldsymbol{s}}_{\oplus,k}}{\left\|{}^{\mathcal{N}}\hat{\boldsymbol{r}}_{A_jB}\right\|^2 \left\|{}^{\mathcal{N}}\boldsymbol{s}_{\oplus,k}\right\|} \left({}^{\mathcal{N}}\boldsymbol{n}_{A_j}^T \frac{{}^{\mathcal{N}}\hat{\boldsymbol{r}}_{A_jB}}{\left\|{}^{\mathcal{N}}\hat{\boldsymbol{r}}_{A_jB}\right\|} \right) \\ \quad \left({}^{\mathcal{N}}\boldsymbol{n}_i^T \frac{{}^{\mathcal{N}}\hat{\boldsymbol{r}}_{A_jB}}{\left\|{}^{\mathcal{N}}\hat{\boldsymbol{r}}_{A_jB}\right\|} \right) \Delta A_j & \text{if } \mathrm{d}A \in \boldsymbol{A} \\ \boldsymbol{0} & \text{if } \mathrm{d}A \notin \boldsymbol{A} \end{cases} \tag{35b}$$

and

$$\boldsymbol{J}_k = \boldsymbol{J}_{d_k} + \boldsymbol{J}_{\alpha_k} \tag{36a}$$

$$\boldsymbol{J}_{d_k} = \begin{bmatrix} \boldsymbol{a}_{1,k} & -\boldsymbol{a}_{1,k} \\ \vdots & \vdots \\ \boldsymbol{a}_{N,k} & -\boldsymbol{a}_{N,k} \end{bmatrix}$$

$$\boldsymbol{a}_{i,k} = \begin{cases} -\hat{C}_{i,k}^{\mathcal{B}} \begin{bmatrix} \cos\phi_i \cos\theta_i & \cos\phi_i \sin\theta_i & \sin\phi_i \end{bmatrix} [BN] \\ \quad * \frac{1}{\left\|{}^{\mathcal{N}}\hat{\boldsymbol{s}}_k\right\|} \left(\boldsymbol{I}_{3\times 3} - \frac{{}^{\mathcal{N}}\hat{\boldsymbol{s}}_k \, {}^{\mathcal{N}}\hat{\boldsymbol{s}}_k^T}{\left\|{}^{\mathcal{N}}\hat{\boldsymbol{s}}_k\right\| \left\|{}^{\mathcal{N}}\hat{\boldsymbol{s}}_k\right\|} \right) & \text{if } \frac{\boldsymbol{n}_i^T \hat{\boldsymbol{s}}_k}{\left\|\boldsymbol{n}_i\right\| \left\|\hat{\boldsymbol{s}}_k\right\|} \geq \cos\psi_i \\ 0 & \text{if } \frac{\boldsymbol{n}_i^T \hat{\boldsymbol{s}}_k}{\left\|\boldsymbol{n}_i\right\| \left\|\hat{\boldsymbol{s}}_k\right\|} < \cos\psi_i \end{cases} \tag{36b}$$

$$\boldsymbol{J}_{\alpha,k} = \begin{bmatrix} \boldsymbol{a}_{1,k} & \boldsymbol{b}_{1,k} \\ \vdots & \vdots \\ \boldsymbol{a}_{N,k} & \boldsymbol{b}_{N,k} \end{bmatrix}, \quad (\cdot)_{i,k} = \begin{cases} (\bar{\cdot})_{i,k} & \text{if } B \notin \boldsymbol{\mathcal{S}} \\ \boldsymbol{0} & \text{if } B \in \boldsymbol{\mathcal{S}} \end{cases}$$

$$\bar{\boldsymbol{a}}_{i,k} \approx \frac{\hat{C}_{i,k}}{\pi} \iint_{\boldsymbol{A}} \frac{\alpha}{\left\|{}^{\mathcal{N}}\hat{\boldsymbol{r}}_{AB,k}\right\|^2 \left\|{}^{\mathcal{N}}\hat{\boldsymbol{s}}_{\oplus,k}\right\|} {}^{\mathcal{N}}\boldsymbol{n}_A^T \left(\boldsymbol{I}_{3\times 3} - \frac{{}^{\mathcal{N}}\hat{\boldsymbol{s}}_{\oplus,k} \, {}^{\mathcal{N}}\hat{\boldsymbol{s}}_{\oplus,k}^T}{\left\|{}^{\mathcal{N}}\hat{\boldsymbol{s}}_{\oplus,k}\right\| \left\|{}^{\mathcal{N}}\hat{\boldsymbol{s}}_{\oplus,k}\right\|} \right) \left({}^{\mathcal{N}}\boldsymbol{n}_A^T \frac{{}^{\mathcal{N}}\hat{\boldsymbol{r}}_{AB,k}}{\left\|{}^{\mathcal{N}}\hat{\boldsymbol{r}}_{AB,k}\right\|} \right) \left({}^{\mathcal{N}}\boldsymbol{n}_i^T \frac{{}^{\mathcal{N}}\hat{\boldsymbol{r}}_{AB,k}}{\left\|{}^{\mathcal{N}}\hat{\boldsymbol{r}}_{AB,k}\right\|} \right) \mathrm{d}A$$

$$\begin{aligned} \bar{\boldsymbol{b}}_{i,k} \approx -\frac{\hat{C}_{i,k}}{\pi} \iint_{\boldsymbol{A}} \alpha \frac{{}^{\mathcal{N}}\boldsymbol{n}_A^T \, {}^{\mathcal{N}}\hat{\boldsymbol{s}}_{\oplus,k}}{\left\|{}^{\mathcal{N}}\hat{\boldsymbol{r}}_{AB,k}\right\|^3 \left\|{}^{\mathcal{N}}\hat{\boldsymbol{s}}_{\oplus,k}\right\|} \Bigg[& 2 \frac{{}^{\mathcal{N}}\hat{\boldsymbol{r}}_{AB,k}^T}{\left\|{}^{\mathcal{N}}\hat{\boldsymbol{r}}_{AB,k}\right\|} \left({}^{\mathcal{N}}\boldsymbol{n}_A^T \frac{{}^{\mathcal{N}}\hat{\boldsymbol{r}}_{AB,k}}{\left\|{}^{\mathcal{N}}\hat{\boldsymbol{r}}_{AB,k}\right\|} \right) \left({}^{\mathcal{N}}\boldsymbol{n}_i^T \frac{{}^{\mathcal{N}}\hat{\boldsymbol{r}}_{AB,k}}{\left\|{}^{\mathcal{N}}\hat{\boldsymbol{r}}_{AB,k}\right\|} \right) \\ & - {}^{\mathcal{N}}\boldsymbol{n}_A^T \left(\boldsymbol{I}_{3\times 3} - \frac{{}^{\mathcal{N}}\hat{\boldsymbol{r}}_{AB,k} \, {}^{\mathcal{N}}\hat{\boldsymbol{r}}_{AB,k}^T}{\left\|{}^{\mathcal{N}}\hat{\boldsymbol{r}}_{AB,k}\right\|^2} \right) \left({}^{\mathcal{N}}\boldsymbol{n}_i^T \frac{{}^{\mathcal{N}}\hat{\boldsymbol{r}}_{AB,k}}{\left\|{}^{\mathcal{N}}\hat{\boldsymbol{r}}_{AB,k}\right\|} \right) \\ & - \left({}^{\mathcal{N}}\boldsymbol{n}_A^T \frac{{}^{\mathcal{N}}\hat{\boldsymbol{r}}_{AB,k}}{\left\|{}^{\mathcal{N}}\hat{\boldsymbol{r}}_{AB,k}\right\|} \right) {}^{\mathcal{N}}\boldsymbol{n}_i^T \left(\boldsymbol{I}_{3\times 3} - \frac{{}^{\mathcal{N}}\hat{\boldsymbol{r}}_{AB,k} \, {}^{\mathcal{N}}\hat{\boldsymbol{r}}_{AB,k}^T}{\left\|{}^{\mathcal{N}}\hat{\boldsymbol{r}}_{AB,k}\right\|^2} \right) \Bigg] \mathrm{d}A \end{aligned} \tag{36c}$$

where the partial derivative of the DCM $[BN]$ multiplied by some 3×1 vector $\boldsymbol{a}$ with respect to

the MRP attitude $\boldsymbol{\sigma}$ is given by

$$\frac{\partial}{\partial \boldsymbol{\sigma}}\left([BN]\,\boldsymbol{a}\right)\Big|_{\hat{\boldsymbol{\sigma}}} = \frac{8}{\left(1+\hat{\sigma}^2\right)^3}\Bigg[\left(1+\hat{\sigma}^2\right)\Bigg\{\left(-\left[\hat{\boldsymbol{\sigma}}\right]_\times + \frac{1}{2}\left(1-\hat{\sigma}^2\right)\boldsymbol{I}_{3\times 3}\right)\left[\boldsymbol{a}\right]_\times - \left[\hat{\boldsymbol{\sigma}}\times\boldsymbol{a}\right]_\times + \left(\hat{\boldsymbol{\sigma}}\times\boldsymbol{a}\right)\hat{\boldsymbol{\sigma}}^T\Bigg\} + 4\left(-\left[\hat{\boldsymbol{\sigma}}\right]_\times + \frac{1}{2}\left(1-\hat{\sigma}^2\right)\boldsymbol{I}_{3\times 3}\right)\left(\hat{\boldsymbol{\sigma}}\times\boldsymbol{a}\right)\hat{\boldsymbol{\sigma}}^T\Bigg]. \tag{37}$$

Note that some of the Jacobians associated with V_α are approximate. Because V_α involves an area integral

$$V_\alpha = \iint_{\boldsymbol{A}} f\,\mathrm{d}A \tag{38}$$

its partial derivative is found using Leibniz's rule[17]

$$\frac{\partial V_\alpha}{\partial \boldsymbol{x}} = \iint_{\boldsymbol{A}} \frac{\partial f}{\partial \boldsymbol{x}}\,\mathrm{d}A + \left[f\frac{\partial A}{\partial \boldsymbol{x}}\right]_{\boldsymbol{\mathcal{C}_A}} \tag{39}$$

where $\boldsymbol{\mathcal{C}_A}$ is the bounding contour of the area $\boldsymbol{A}$. The variation of f with respect to the state vector is included in the Jacobians given previously, but the variations of the area being integrated with respect to the state vector are not. Because the definition of $\boldsymbol{A}$ is dependent on $\boldsymbol{\sigma}$, $\boldsymbol{\theta}$, $\boldsymbol{\phi}$, $\boldsymbol{s}_{\oplus_\beta}$, and $\boldsymbol{r}_{B_\beta}$ the second term in Equation (39) needs to be included. However, due to the discrete, and highly uncertain, nature of the albedo data and the complexity of the definition of the bounding contour of $\boldsymbol{A}$, this calculation becomes extremely complex and the associated error in not including it is small. Instead the associated error is accounted for by inflating v_v and verifying through Monte Carlo analysis.

Reduced CSS Calibration Filter

The minimal CSS calibration filter assumes the spacecraft has CSS, inertial attitude, angular rate measurements, and an estimate of the current time for calculating a reference Earth-Sun vector. In contrast to the full CSS calibration filter, it is assumed the received irradiance due to Earth's albedo is treated as an unmodeled measurement bias. This method aims to reduce the total computation time, at the cost of estimation accuracy, by eliminating the costly evaluation of the irradiance contributions caused by the Earth's albedo*. A continuous-discrete extended consider Kalman filter is used again and the state and process noise vectors are unchanged, along with the attitude measurement update, from the full CSS calibration filter.

Because the input irradiance due to Earth's albedo is treated as a bias, Equation (32) is modified to

$$V = C\left(V_d + V_\alpha + \nu_V\right)$$
$$V_d = \begin{cases} {}^{\mathcal{B}}\Big[\cos\phi\cos\theta \quad \cos\phi\sin\theta \quad \sin\phi\Big]\,[BN]\,\frac{{}^{\mathcal{N}}\boldsymbol{s}_\oplus - {}^{\mathcal{N}}\boldsymbol{r}_B}{\left\|{}^{\mathcal{N}}\boldsymbol{s}_\oplus - {}^{\mathcal{N}}\boldsymbol{r}_B\right\|} & \text{if } \boldsymbol{n}^T\frac{\boldsymbol{s}}{\|\boldsymbol{s}\|} \geq \cos\psi \\ 0 & \text{if } \boldsymbol{n}^T\frac{\boldsymbol{s}}{\|\boldsymbol{s}\|} < \cos\psi \end{cases} \tag{40}$$

*Evaluating the full NASA TOMS albedo model involves looping through $51\,840$ elements, for each of the CSS, every measurement update and possibly evaluating several equations at each element; a process which can take significant time as shown later in the results.

and the measurement noise and bias vectors are changed to

$$\boldsymbol{\nu}_k = \begin{bmatrix}\boldsymbol{\nu}_{V,k}\end{bmatrix}, \quad \boldsymbol{\beta}_\nu = \begin{bmatrix} {}^{\mathcal{N}}\boldsymbol{s}_{\oplus_\beta,k} \\ {}^{\mathcal{N}}\boldsymbol{r}_{B_\beta,k} \\ \boldsymbol{V}_{\alpha_\beta,k} \end{bmatrix} \tag{41}$$

where, without an orbit solution, the spacecraft position relative to the Earth is treated as a systematic bias. It is expected that this bias will have minimal impact on the estimate, especially when compared to the effect of Earth's albedo.

The measurement update Jacobians are given by Equation (34), where now $\boldsymbol{H}_{\alpha,k} = \mathbf{0}$,

$$\boldsymbol{M}_k = \operatorname{diag}\left(\hat{\boldsymbol{C}}_k^T\right) \tag{42}$$

and

$$\boldsymbol{J}_k = \begin{bmatrix} \begin{bmatrix}\boldsymbol{a}_{1,k}\\ \vdots \\ \boldsymbol{a}_{N,k}\end{bmatrix} & \begin{bmatrix}\boldsymbol{a}_{1,k}\\ \vdots \\ \boldsymbol{a}_{N,k}\end{bmatrix} & \operatorname{diag}\left(\hat{\boldsymbol{C}}_k^T\right) \end{bmatrix}$$

$$\boldsymbol{a}_{i,k} = \begin{cases} -\hat{C}_{i,k}\,{}^{\mathcal{B}}\begin{bmatrix}\cos\phi_i\cos\theta_i & \cos\phi_i\sin\theta_i & \sin\phi_i\end{bmatrix}[BN] \\ \quad *\frac{1}{\left\|{}^{\mathcal{N}}\hat{\boldsymbol{s}}_k\right\|}\left(\boldsymbol{I}_{3\times3} - \frac{{}^{\mathcal{N}}\hat{\boldsymbol{s}}_k\,{}^{\mathcal{N}}\hat{\boldsymbol{s}}_k^T}{\left\|{}^{\mathcal{N}}\hat{\boldsymbol{s}}_k\right\|\left\|{}^{\mathcal{N}}\hat{\boldsymbol{s}}_k\right\|}\right) & \text{if } \boldsymbol{n}_i^T\frac{\hat{\boldsymbol{s}}_k}{\left\|\hat{\boldsymbol{s}}_k\right\|} \geq \cos\psi_i \\ 0 & \text{if } \boldsymbol{n}_i^T\frac{\hat{\boldsymbol{s}}_k}{\left\|\hat{\boldsymbol{s}}_k\right\|} < \cos\psi_i \end{cases} \tag{43}$$

where, because the nominal value for the bias estimate ${}^{\mathcal{N}}\hat{\boldsymbol{r}}_{B_\beta,k}$ is a zero vector, ${}^{\mathcal{N}}\hat{\boldsymbol{s}}_k \approx {}^{\mathcal{N}}\hat{\boldsymbol{s}}_{\oplus,k}$.

NUMERICAL SIMULATION

A spacecraft is modeled in a $400\,\mathrm{km}$ altitude circular orbit with an inclination of 90° starting on 2015 June 1, 00:00 UTC. The simulation is run for one orbit from when the spacecraft first sees the Sun until it returns to the shadow of the Earth. The accelerations due to the J_2 through J_6 Earth zonal gravitational perturbations, atmospheric drag, and solar radiation pressure (SRP) are modeled. The relative positions of the Earth and Sun are simulated using ephemeris from the NASA Navigation and Ancillary Information Facility (NAIF) SPICE toolkit.[18] The spacecraft is assumed to have a mass of $100\,\mathrm{kg}$, a drag area of approximately $0.38\,\mathrm{m}^2$, a ballistic coefficient of 2.1, a cross sectional area of $1.3\,\mathrm{m}^2$ subject to SRP, and an inertia matrix given by $[I] = \operatorname{diag}\begin{bmatrix}10.5 & 8.0 & 6.75\end{bmatrix}\mathrm{kg\,m}^2$. The spacecraft is simulated in an uncontrolled tumble, but calibration can be reliably performed with Nadir pointing control active, or a similar maneuver in which each sensor is pointed at the Sun at some point in the orbit.

The spacecraft's initial attitude is $\boldsymbol{\sigma} = [-0.06166, -0.43080, -0.15439]$ and its initial angular velocity is $\boldsymbol{\omega} = [-0.55989, -0.97885, 1.94116]^\circ\,\mathrm{s}^{-1}$. Rate gyroscope measurements are simulated at $10\,\mathrm{Hz}$, the rate white noise standard deviation is assumed to be $0.05\,^\circ/\sqrt{\mathrm{h}}$ with a drift stability standard deviation of $0.5\,^\circ\,\mathrm{h}^{-1}$ over $1000\,\mathrm{s}$. Star tracker measurements are simulated at $2\,\mathrm{Hz}$ and corrupted by white Gaussian noise with a standard deviation of 20 arcseconds. Orbit position measurements are simulated at $1\,\mathrm{Hz}$ corrupted by position errors with a standard deviation of $1\,\mathrm{km}$ and velocity errors with a standard deviation of $0.1\,\mathrm{km\,s}^{-1}$ about each axis.

The alignment azimuth and elevation of each CSS is perturbed by a normally distributed angle with a standard deviation of 1°. All CSS are assumed to have calibration scale factors normally distributed by $30\,\%$, 1σ, from a nominal calibration scale factor of $C = 1.0$. As noted in the introduction, this represents a significant variation. CSS measurements are processed at $2\,\mathrm{Hz}$ and white Gaussian noise is added to each sensor with a standard deviation of 0.05. The full $1^\circ \times 1.25^\circ$ latitude longitude grid of albedo values is used to calculate the reference Earth albedo.

Comparison of Albedo Models

The full and reduced calibration filters are compared along with the full calibration filter run using lower resolution albedo data sets. The full calibration filter is run using a $1^\circ \times 1.25^\circ$, $5^\circ \times 5^\circ$, and $10^\circ \times 10^\circ$ resolution albedo data sets, where the lower resolution grids are interpolated from the $1^\circ \times 1.25^\circ$ data. It was found through Monte Carlo analysis that the measurement noise ν_V needs to be raised from 0.05, as determined by the CSS noise, to 0.1 for the $1^\circ \times 1.25^\circ$ albedo grid, to 0.175 for the $5^\circ \times 5^\circ$ albedo grid, and to 0.3 for the $10^\circ \times 10^\circ$ albedo grid in order to account for the unmodeled aspects of the partial derivatives.

The estimation errors and 3σ uncertainty bounds are shown in Figures 3 and 4. As can be seen in Figure 3, all of the estimators calculate attitude and rate gyro bias estimates within the computed 3σ uncertainty bounds. The error in these parameters is relatively small and is driven by the accuracy of the star tracker. The impact of the CSS measurements on the attitude estimate is so small the differences between methods is indistinguishable at the scale displayed. Because of this, computation could be saved if a spacecraft already has an attitude estimator by substituting in the estimated attitude and rate gyro bias from the attitude estimator into the calibration filter.

For brevity, only the calibration estimates for CSS 2 and 6 are shown in Figure 4. These two CSS are shown as they represent the least and most observable sensors for the particular tumble the spacecraft is simulated in, and they are representative of the output of all the sensor calibration parameters. As can be seen, the calibration coefficient C is much more observable than the misalignments of the individual sensors. Additionally, using even a very coarse albedo data set within the estimator provides significant improvement over treating the irradiance due to albedo as a bias. For the reduced filter the uncertainty in CSS 2's calibration coefficient C is reduced to 0.14, 3σ, in just one orbit. The full filter with $10^\circ \times 10^\circ$ albedo data reduces that to 0.02, and using the full $1^\circ \times 1.25^\circ$ albedo data that value is decreased to 0.008. It is shown in References 7 and 8 that with scale factor uncertainty of 0.06, 3σ, simultaneous coarse sun-direction estimation and control to within $10\,\mathrm{degree}$ can be achieved in just a few minutes from an unknown tumbling attitude. Similar trends are seen in the alignment angles θ and ϕ with the full calibration filter uncertainty at least a full degree less than the reduced calibration filter. All four methods reduce the uncertainty in the alignment angles below the values used in References 7 and 8, showing that sufficient calibration for sun-pointing can be achieved with reduced effort.

To compare the computation time for these algorithms the propagation and measurement update algorithms are timed and recorded. For the $3460\,\mathrm{s}$ simulation the propagation update is called $34\,601$ times and the estimation update 6921 times. The execution time for each algorithm is recorded each of these times and the averages and standard deviations are shown in Table 1. The simulations followed exactly the same trajectory and experienced identical simulated sensor measurements. The propagation algorithms are coded exactly the same except for the size of the bias covariance matrices. The measurement update equations are coded exactly the same with two exceptions: the full calibration filter includes a loop over the albedo data to calculate the expected irradiance due to

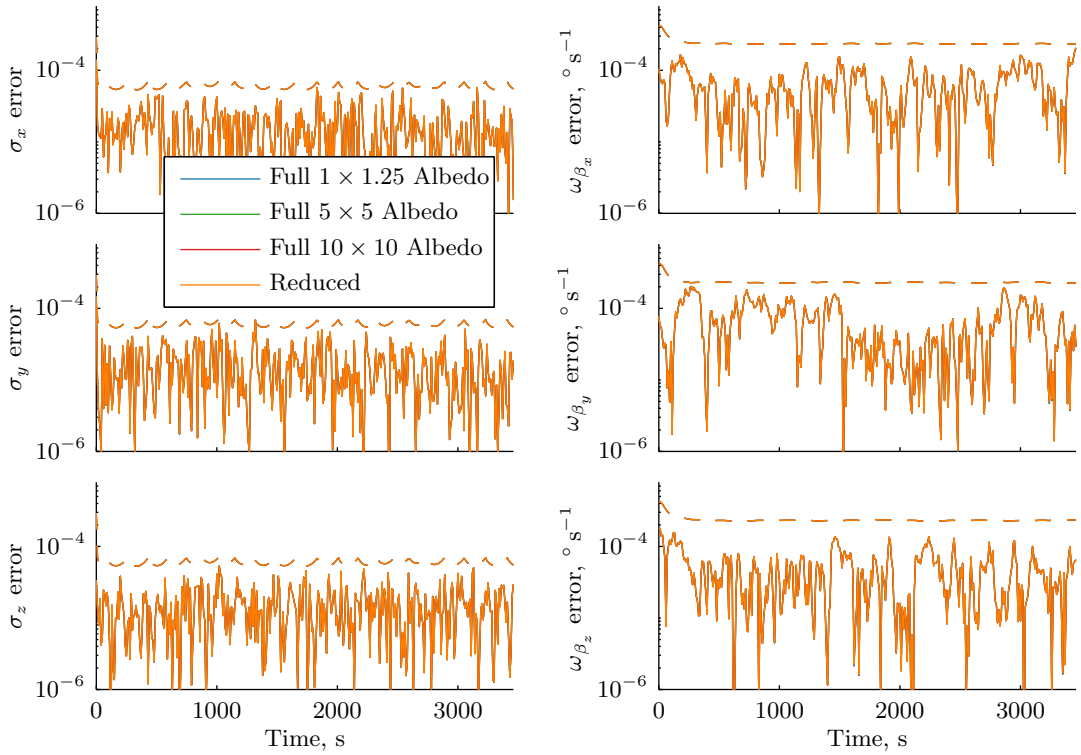

(a) Error in MRP attitude.

(b) Error in rate gyro bias.

Figure 3: Calculated mean (solid) and 3σ (dashed) MRP and rate gyro bias values for full and reduced estimation techniques.

albedo and the associated uncertainties; and the matrix sizes of the bias covariance matrices have different dimensions between the full and reduced calibration filters. All code was written in C and compiled and run on a Windows i7 2.5 GHz computer. While this is not flight hardware, the relative computation times are what are important.

Table 1: Averages and standard deviations for computation times of various filters.

ECKF	Albedo Data	Propagation Update, µs	Measurement Update, µs
Full	$1^\circ \times 1.25^\circ$	14.7 ± 1.5	5868 ± 1397
Full	$5^\circ \times 5^\circ$	13.8 ± 1.8	522 ± 90.4
Full	$10^\circ \times 10^\circ$	14.6 ± 1.2	228 ± 21.3
Reduced	-	17.0 ± 1.9	278 ± 29.0

As expected reducing the density of the albedo grid greatly increases the computation speed. Interestingly, the computation time for the 10×10 albedo grid is lower than that of the reduced calibration filter. This is a result of the total mathematical operations performed. Comparing Equations (33) and (41) it can be seen that the reduced calibration filter trades the computation of the albedo, and its associated uncertainty, for an increased number of bias parameters, whose uncertainty and correlation with the state must be propagated and updated. For a low resolution albedo

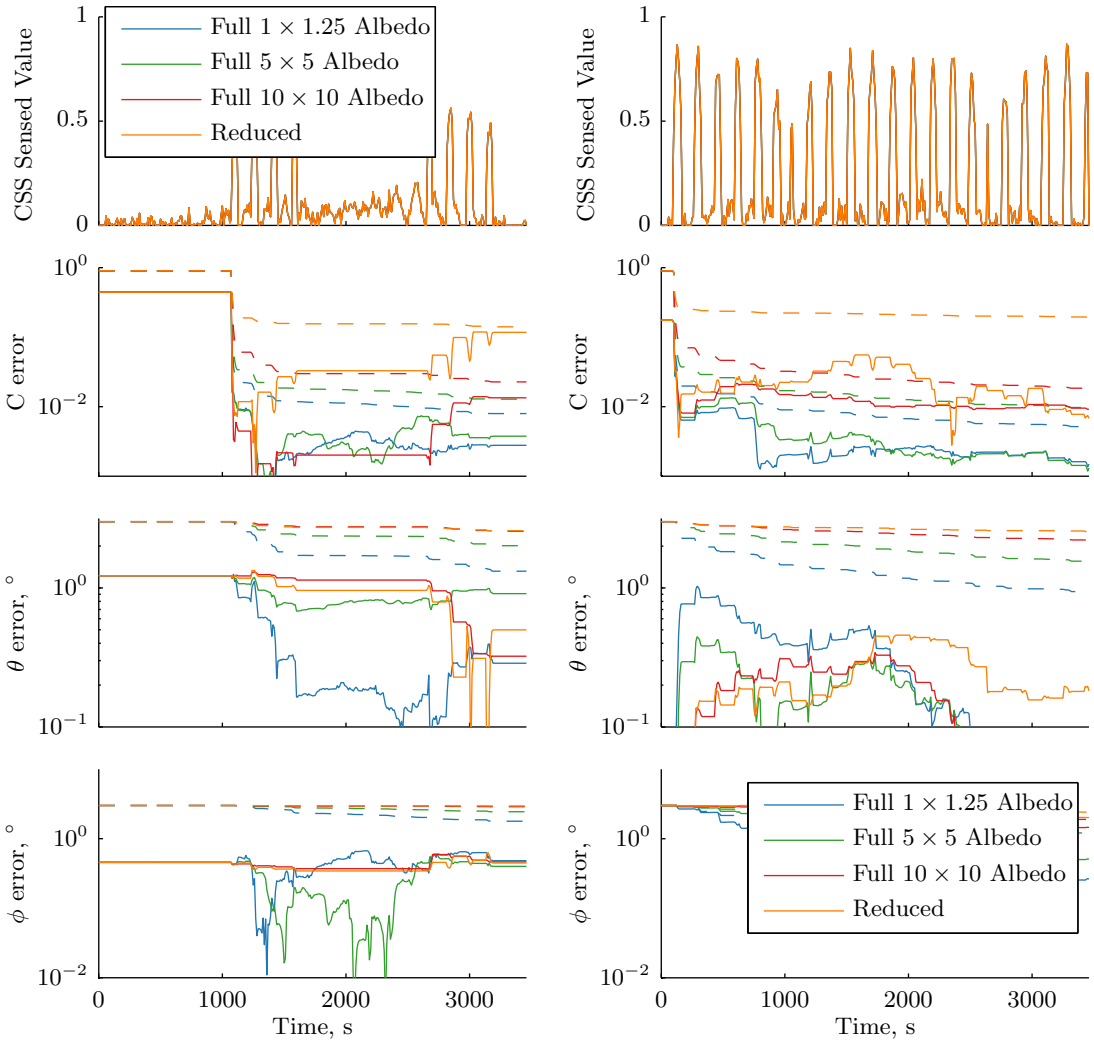

(a) CSS 2.

(b) CSS 6.

Figure 4: Calculated mean (solid) and 3σ (dashed) CSS calibration values for full and reduced estimation techniques for CSS 2 and 6.

dataset the number of computations necessary to loop through the albedo data will eventually drop below the number of calculations added by accounting for the albedo as a measurement bias in the ECKF formulation. For the current state vector this break even point occurs near an albedo resolution of $10^\circ \times 10^\circ$.

Comparison of Sun-Direction Models

There are several methods available for computing the direction vector from the Earth to the Sun based on only a reference time depending on the computational power available and accuracy desired. When calculating a normalized sun-direction vector in the body frame of a spacecraft in low Earth orbit these methods provide a relatively small level of error. Vallado gives an analytic method valid from 1950 to 2050.[19] *Variations Séculaires des Orbites Planétaires* (VSOP) provides

a series of periodic terms that can be used to determine the position of the planets.[20] Meeus provides an abbreviated set of VSOP87 tables and associated algorithm.[21] Finally, the NASA Navigation and Ancillary Information Facility (NAIF) SPICE toolkit provides full planetary ephemerides.[18]

Vallado's method takes less time to evaluate at the cost of accuracy. When compared to the NASA SPICE toolkit, the method provided by Vallado has maximum errors of $1.33 \times 10^{-6}\,\mathrm{km}$, $1.33 \times 10^{-6}\,\mathrm{km}$, and $0.66 \times 10^{-3}\,\mathrm{km}$ about the x, y, and z axes, respectively; and the remaining methods have a maximum error of $1 \times 10^{-6}\,\mathrm{km}$ about each axis. Expressed alternatively, the error in Vallado's method corresponds approximately to an input time error of $6\,\mathrm{h}$ using the other algorithms. The full calibration algorithm was run nominally using Meeus' algorithm, but is run here with Vallado's algorithm for comparison, and the results are shown in Figure 5. Additionally included is a case in which the orbit knowledge error is increased by an order of magnitude in position and velocity.

As can be seen, the estimated uncertainty bounds have very little dependence on the sun-direction model used or the orbit accuracy. The propagation update computation time is unchanged when switching to Vallado's sun-direction model, and the measurement update is only sped up by $10\,\mu\mathrm{s}$, on average, which is small compared to the total measurement update time of several hundred microseconds.

CONCLUSION

An MRP-based CSS calibration filter, based on an extended consider Kalman filter, is presented for estimating the calibration coefficient and alignment misalignment angles of CSS onboard a spacecraft in low Earth orbit. The full filter uses orbit knowledge to compute the irradiance contributions to each CSS due to Earth's albedo. A reduced filter is also presented that doesn't require orbit knowledge and a a consequence treats the irradiance due to Earth's albedo as an unmodeled bias. The relative accuracies and computation time of these two methods are computed using numerical simulations. It is shown estimation using even a very coarse albedo dataset is superior to treating the albedo as a bias. At best, CSS calibration scale factors can be estimated to less than $1\,\%$ and alignment angles to approximately 1°. However, computation time can be reduced by a factor of 25 and calibration coefficient accuracies of $2\,\%$ and alignment accuracies of approximately 2° can still be achieved. Such a calibration filter could be used onboard a small satellite in order to reduce necessary ground support and increase autonomy.

REFERENCES

[1] P. Appel, "Attitude Estimation from Magnetometer and Earth-Albedo-Corrected Coarse Sun Sensor Measurements," *Acta Astronautica*, Vol. 56, Jan. 2005, pp. 2–5, 10.1016/j.actaastro.2004.09.001.

[2] H. Jung and M. L. Psiaki, "Tests of Magnetometer/Sun-Sensor Orbit Determination Using Flight Data," *Proceedings of the AIAA Guidance, Navigation, and Control Conference and Exhibit*, No. August, Montreal, Canada, American Institute of Aeronautics and Astronautics, Aug. 2001.

[3] J. C. Springmann, "On-Orbit Calibration of Photodiodes for Attitude Determination," *Proceedings of the AIAA/USU Conference on Small Satellites*, Logan, UT, Aug. 2013.

[4] P. Ortega, G. López-Rodríguez, J. Ricart, M. Domínguez, L. M. Castañer, J. M. Quero, C. L. Tarrida, J. García, M. Reina, A. Gras, and M. Angulo, "A Miniaturized Two Axis Sun Sensor for Attitude Control of Nano-Satellites," *IEEE Sensors Journal*, Vol. 10, No. 10, 2010, pp. 1623–1632, 10.1109/JSEN.2010.2047104.

[5] S.-F. Wu and W. H. Steyn, "Modelling and in-orbit calibration practice of a miniature 2-axis analogue sun sensor," *Aerospace Science and Technology*, Vol. 6, Oct. 2002, pp. 423–433, 10.1016/S1270-9638(02)01187-2.

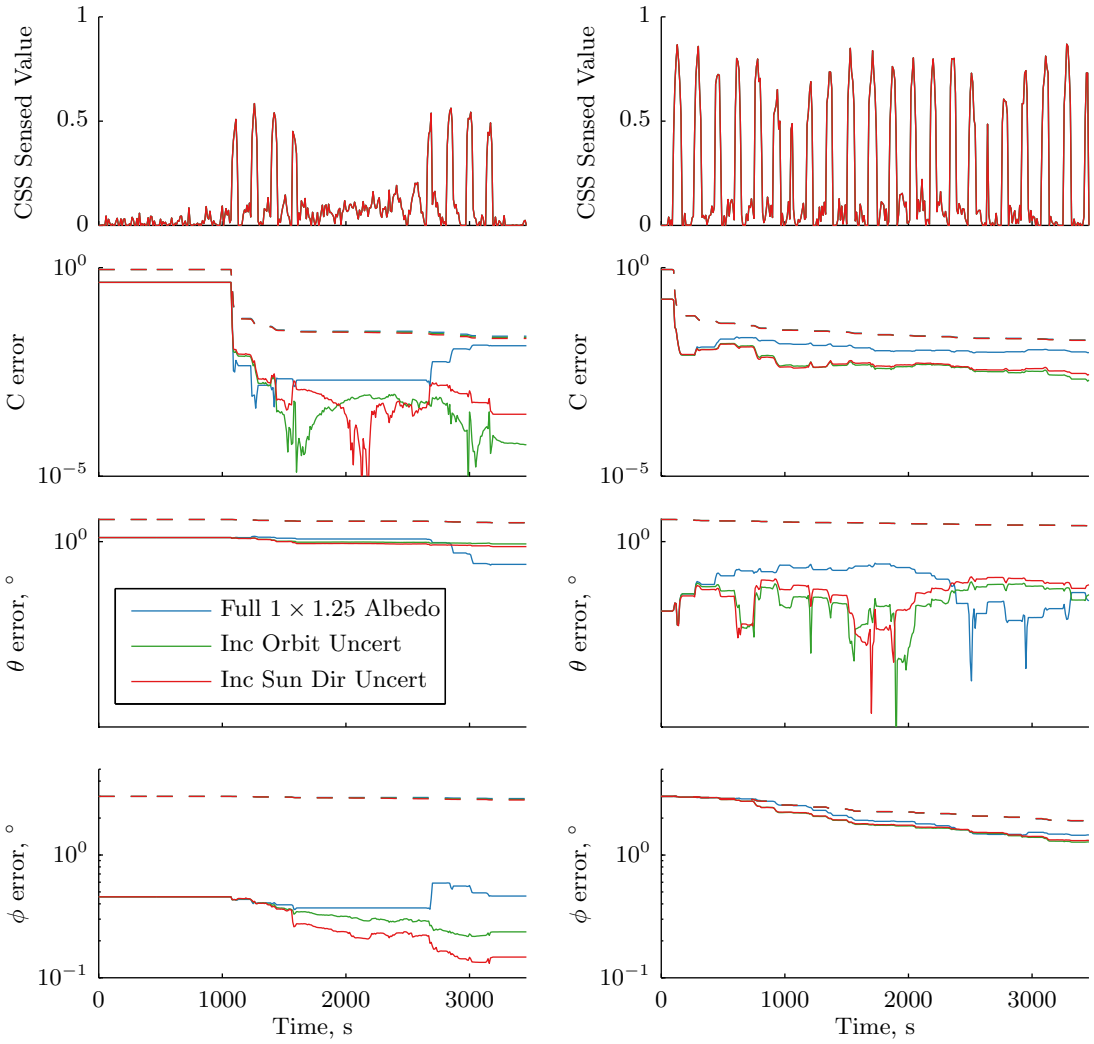

(a) CSS 2.

(b) CSS 6.

Figure 5: Calculated mean (solid) and 3σ (dashed) CSS calibration values for increased orbit and sun-direction uncertainty for CSS 2 and 6.

[6] C. D. Karlgaard and H. Schaub, "Nonsingular Attitude Filtering Using Modified Rodrigues Parameters," *Journal of the Astronautical Sciences*, Vol. 57, No. 4, 2010, pp. 777–791.

[7] S. A. O'Keefe and H. Schaub, "Sun Heading Estimation Using Underdetermined Set of Coarse Sun Sensors," *Proceedings of the AAS/AIAA Astrodynamics Specialist Conference*, Hilton Head, SC, Aug. 2013.

[8] S. A. O'Keefe and H. Schaub, "Gyro Accuracy and Failure Sensitivity of Underdetermined Coarse Sun-Direction Estimation," *Proceedings of the AAS/AIAA Astrodynamics Specialist Conference*, Williamsburg, VA, 2015.

[9] N. a. Krivova, L. E. a. Vieira, and S. K. Solanki, "Reconstruction of solar spectral irradiance since the Maunder minimum," *Journal of Geophysical Research*, Vol. 115, Dec. 2010, 10.1029/2010JA015431.

[10] G. M. Lerner, *Spacecraft Attitude Determination and Control*, ch. Sun Sensors, pp. 155–166. Dordrecht, The Netherlands: D. Reidel Publishing Co., 1978.

[11] D. D. V. Bhanderi and T. Bak, "Modeling Earth Albedo for Satellites in Earth Orbit," *Proceedings of the AIAA Guidance, Navigation, and Control Conference and Exhibit*, San Francisco, CA, American Institute of Aeronautics and Astronautics, Aug. 2005.

[12] J. P. Snyder, *Map Projections: A Working Manual*, pp. 76–85. Geological Survey (U.S.) Professional Paper 1395, 1987.

[13] S. F. Schmidt, "Application of State-Space Methods to Navigation Problems," *Advances in Control Systems*, Vol. 3, 1966, pp. 293–340.

[14] R. Zanetti and R. H. Bishop, "Kalman Filters with Uncompensated Biases," *Journal of Guidance, Control, and Dynamics*, Vol. 35, Jan. 2012, pp. 327–335, 10.2514/1.55120.

[15] D. P. Woodbury and J. L. Junkins, "On the Consider Kalman Filter," *AIAA Guidance, Navigation, and Control Conference*, Toronto, ON, American Institute of Aeronautics and Astronautics, Aug. 2010, 10.2514/6.2010-7752.

[16] R. L. Farrenkopf, "Analytic Steady-State Accuracy Solutions for Two Common Spacecraft Attitude Estimators," *Journal of Guidance, Control, and Dynamics*, Vol. 1, No. 4, 1978, pp. 282–284, 10.2514/3.55779.

[17] H. Flanders, "Differentiation Under the Integral Sign," *The American Mathematical Monthly*, Vol. 80, No. 6, 1973, pp. 615–627.

[18] C. Acton, "Ancillary Data Services of NASA's Navigation and Ancillary Information Facility," *Planetary and Space Science*, Vol. 44, No. 1, 1996, pp. 65–70.

[19] D. A. Vallado, *Fundamentals of Astrodynamics and Applications*. Microcosm Press, 2nd ed., 2004.

[20] P. Bretagnon and G. Francou, "Planetary theories in rectangular and spherical variables - VSOP 87 solutions," *Astronomy \& Astrophysics*, Vol. 202, Aug. 1988, pp. 209–315.

[21] J. Meeus, *Astronomial Algorithms*. Willmann-Bell, Inc, 2 ed., 1998.